Doping and Phase Segregation in Mn^{2+}- and Co^{2+}-Doped Lead Halide Perovskites from ^{133}Cs and ^{1}H NMR Relaxation Enhancement

Dominik J. Kubicki,[a,b] Daniel Prochowicz,[b,c] Arthur C. Pinon,[a] Gabriele Stevanato,[a] Albert Hofstetter,[a] Shaik M. Zakeeruddin,[b] Michael Grätzel,*[b] Lyndon Emsley*[a]

[a]*Laboratory of Magnetic Resonance, Institute of Chemical Sciences and Engineering, Ecole Polytechnique Fédérale de Lausanne (EPFL), CH-1015 Lausanne, Switzerland*
[b]*Laboratory of Photonics and Interfaces, Institute of Chemical Sciences and Engineering, Ecole Polytechnique Fédérale de Lausanne (EPFL), CH-1015 Lausanne, Switzerland*
[c]*Institute of Physical Chemistry, Polish Academy of Sciences, Kasprzaka 44/52, 01-224 Warsaw, Poland*

Table of contents

List of figures and tables

XRD patterns

Diffractograms were recorded on an X'Pert MPD PRO (Panalytical) diffractometer equipped with a ceramic tube (Cu anode, λ = 1.54060 Å), a secondary graphite (002) monochromator and an RTMS X'Celerator (Panalytical) in an angle range of 2θ = 5° to 40°, by step scanning with a step of 0.02 degree.

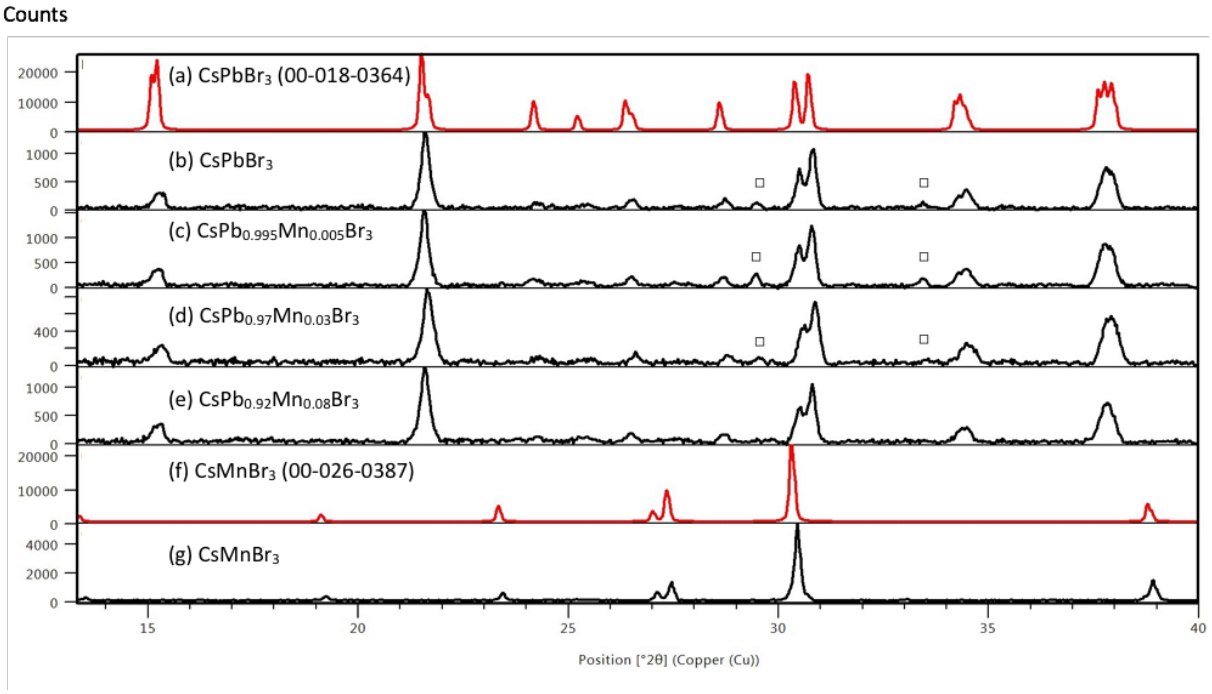

Figure S1. XRD patterns of the materials reported in the main text. Simulated patterns: (a) $CsPbBr_3$ (ICDD: #00-018-0364), (f) $CsMnBr_3$ (ICDD: #00-026-0387). Experimental patterns of mechanochemical perovskite preparations: (b) $CsPbBr_3$, (c) $CsPb_{0.995}Mn_{0.005}Br_3$, (d) $CsPb_{0.97}Mn_{0.03}Br_3$, (e) $CsPb_{0.92}Mn_{0.08}Br_3$, (g) $CsMnBr_3$. □ indicates an impurity. For c, d and e, to within error, there is no measurable shift of the main perovskite peaks with respect to the undoped $CsPbBr_3$. The numbers given in parentheses are ICDD database reference codes.

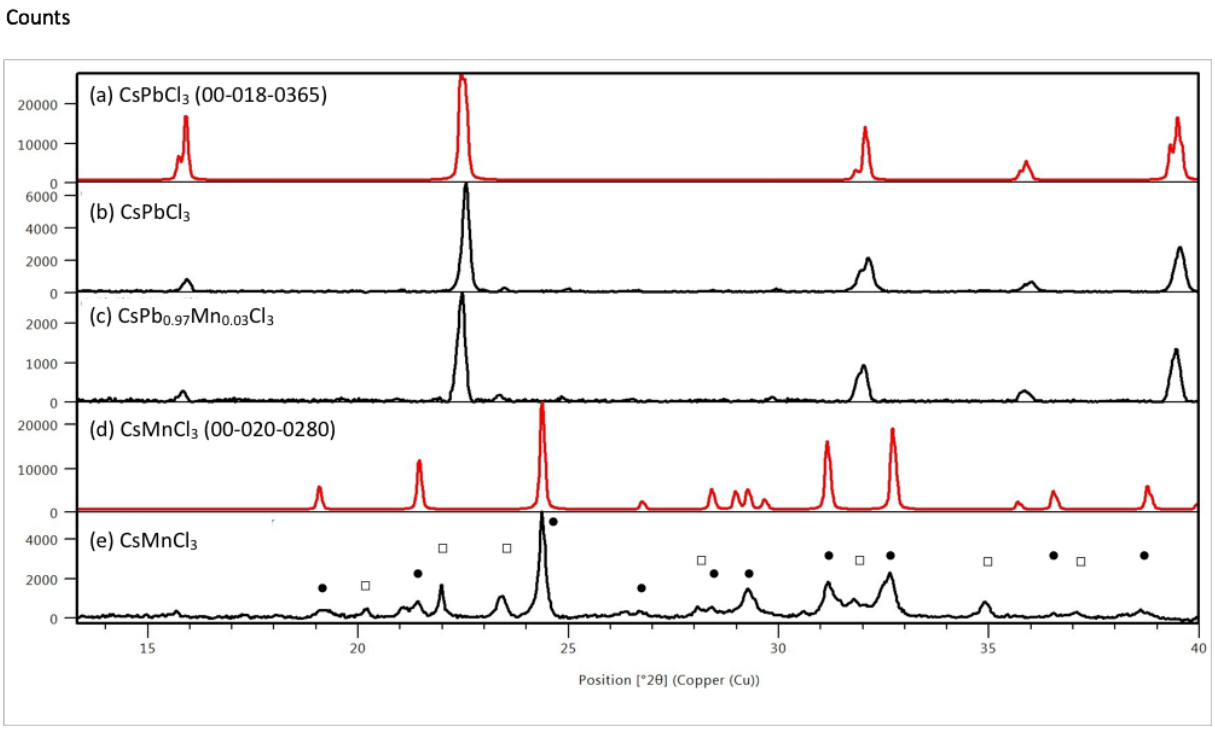

Figure S2. XRD patterns of the materials reported in the main text. Simulated patterns: (a) $CsPbCl_3$ (ICDD: #00-018-0365), (d) $CsMnCl_3$ (ICDD: #00-020-0280). Experimental patterns of mechanochemical perovskite preparations: (b) $CsPbCl_3$, (c) $CsPb_{0.97}Mn_{0.03}Cl_3$, (d) $CsMnCl_3$. $CsMnCl_3$ (indicated as •) contains an impurity phase (indicated as □). To within error, there is no measurable shift of the main perovskite peaks in $CsPb_{0.97}Mn_{0.03}Cl_3$ with respect to the undoped $CsPbCl_3$. The numbers given in parentheses are ICDD database reference codes.

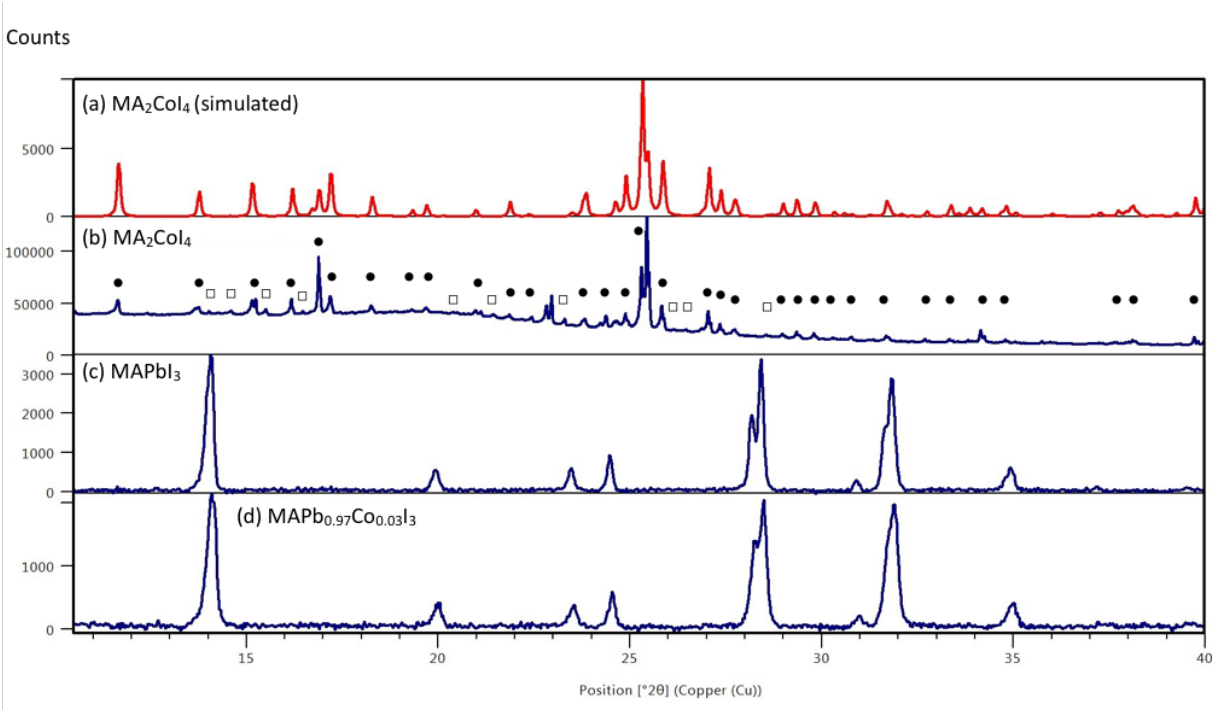

Figure S3. XRD patterns of the materials reported in the main text. Simulated pattern: (a) MA_2CoI_4 (simulated based on a previously reported crystal structure[1]). Experimental

patterns of mechanochemical perovskite preparations: (b) MA_2CoI_4 (indicated as •) (c) $MAPbI_3$, (d) $MAPb_{0.97}Co_{0.03}I_3$. Mechanochemical MA_2CoI_4 contains an impurity phase (indicated as □). To within error, there is no measurable shift of the main perovskite peaks in $MAPb_{0.97}Co_{0.03}I_3$ with respect to the undoped $MAPbI_3$.

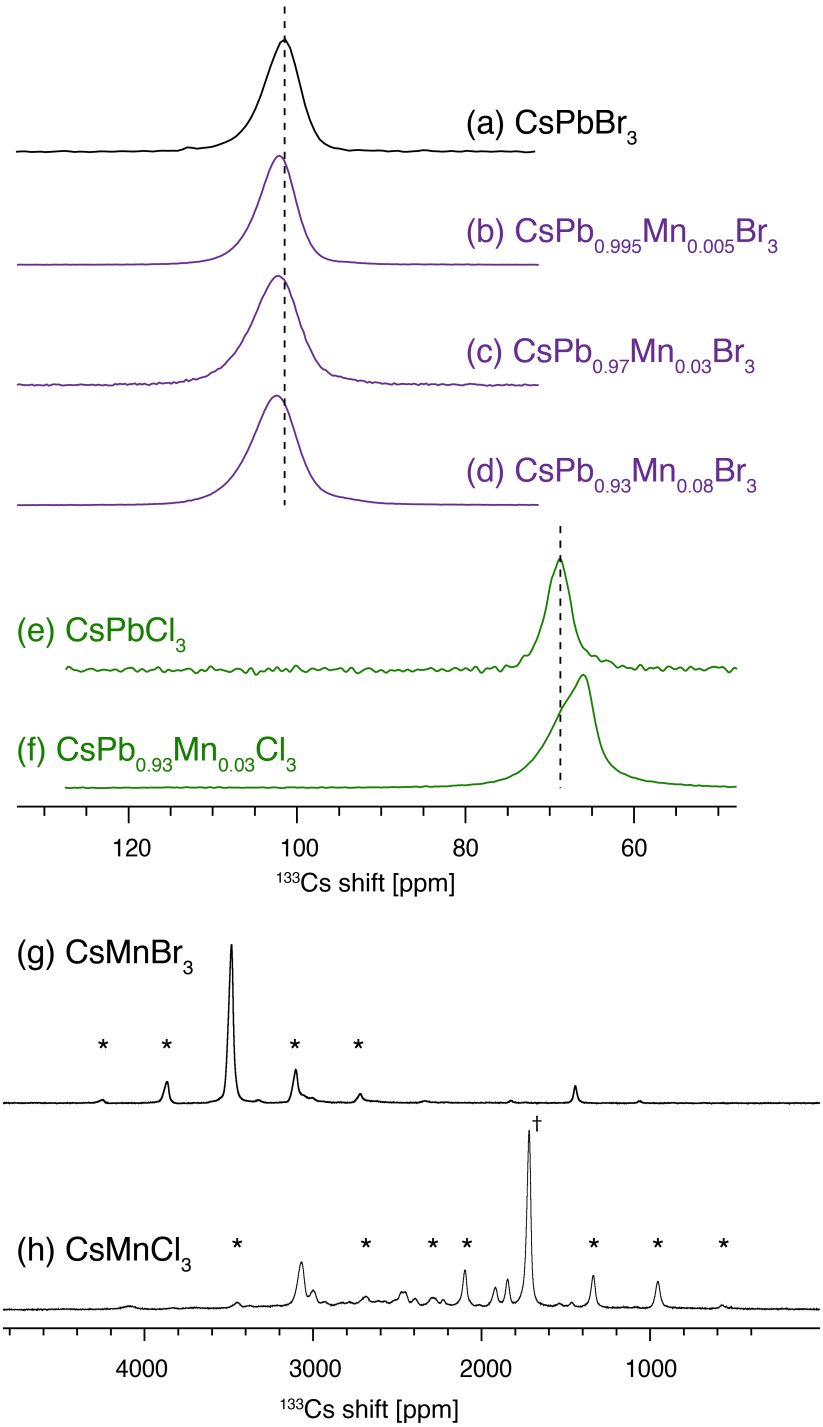

Figure S4. ^{133}Cs NMR spectra at 9.4 T, 20 kHz MAS and 298 K of the materials reported in the main text: (a) $CsPbBr_3$, (b) $CsPb_{0.995}Mn_{0.005}Br_3$, (c) $CsPb_{0.97}Mn_{0.03}Br_3$, (d) $CsPb_{0.92}Mn_{0.08}Br_3$, (e) $CsPbCl_3$, (f) $CsPb_{0.97}Mn_{0.03}Cl_3$, (g) $CsMnBr_3$ (h) $CsMnCl_3$. † indicates the peak on which the saturation-recovery experiment was performed, * indicate spinning sidebands.

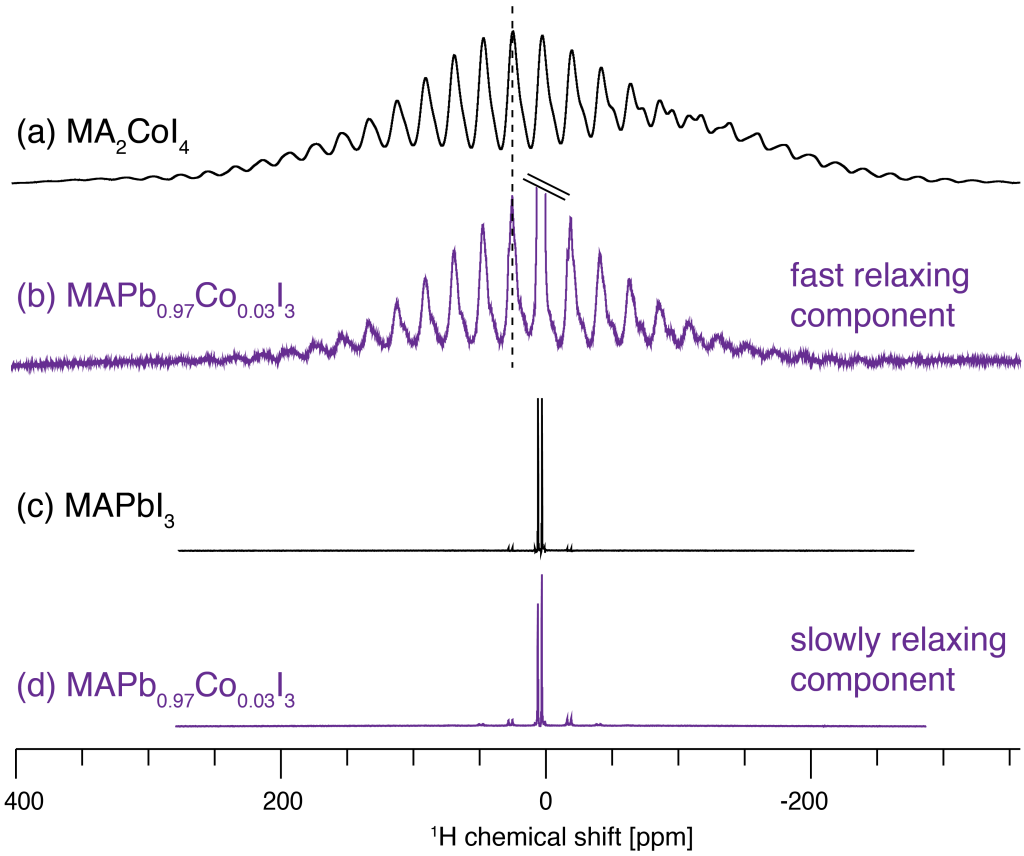

Figure S5. ^{1}H NMR spectra at 21.1 T, 20 kHz MAS and 298 K of the materials reported in the main text: (a) MA_2CoI_4 (recycle delay: 0.001 s, 15265 scans), (b) $MAPb_{0.97}Co_{0.03}I_3$ (recycle delay: 0.001 s to selectively detect the paramagnetic component, 5248 scans), (c) $MAPbI_3$, (recycle delay: 20 s, 4 scans), (b) $MAPb_{0.97}Co_{0.03}I_3$ (recycle delay: 10 s to selectively detect the diamagnetic component, 8 scans). The isotropic peak of the paramagnetic phase in $MAPb_{0.97}Co_{0.03}I_3$ matches perfectly that of the reference MA_2CoI_4 (δ=24.7 ppm).

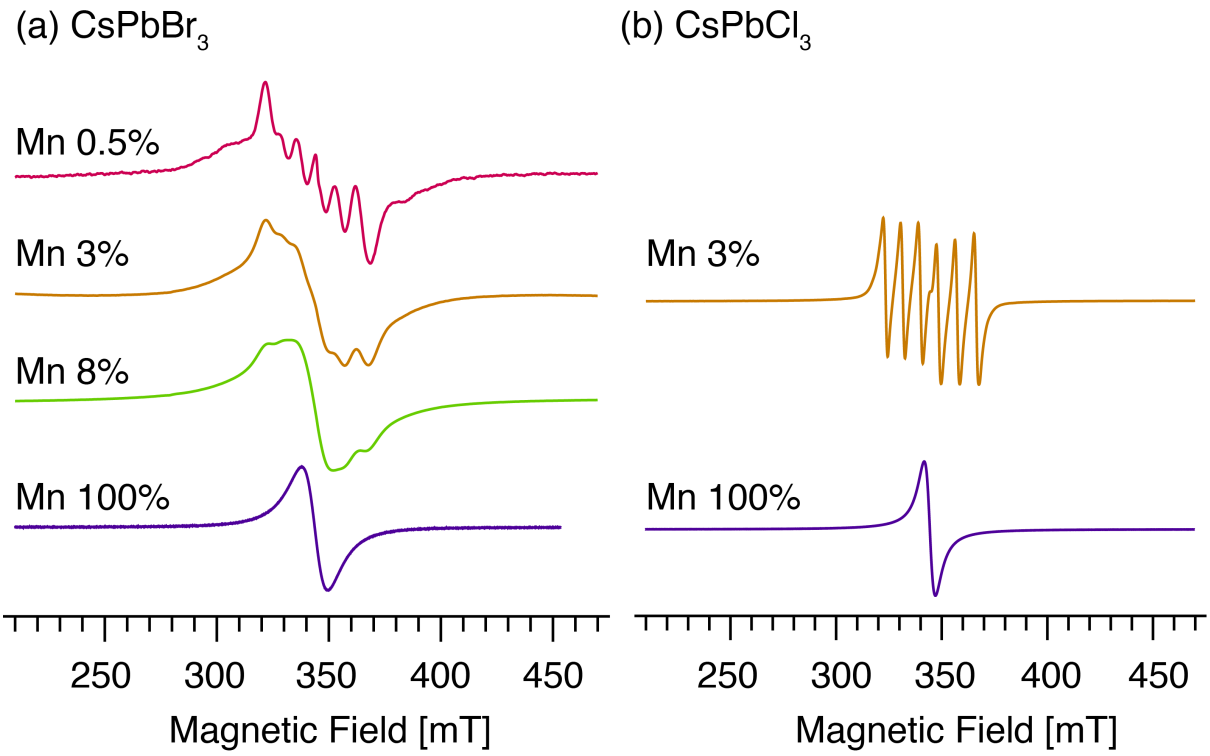

Figure S6. X-band (9.65 GHz) EPR spectra at 298 K of the (a) $CsPbBr_3$- and (b) $CsPbCl_3$-derived materials. Shorthand legend labels are given in parentheses: (a) $CsPb_{0.995}Mn_{0.005}Br_3$ ("Mn 0.5%"), $CsPb_{0.97}Mn_{0.03}Br_3$ ("Mn 3%"), $CsPb_{0.92}Mn_{0.08}Br_3$ ("Mn 8%") and $CsMnBr_3$ ("Mn 100%"), (b) $CsPb_{0.97}Mn_{0.03}Cl_3$ ("Mn 3%") and $CsMnCl_3$ ("Mn 100%").

Polarisation dynamics

The general model used to fit experimental data shown in the main text is based on the propagation of PRE by spin diffusion. Polarization dynamics follows a behaviour similar to heat transfer which can be described by the following equation[2]:

$$C_{Cs}(x) \cdot \frac{\partial P(x,t)}{\partial t} = \nabla(D_{Cs}(x) \cdot C_{Cs}(x) \cdot \nabla P(x,t)) - C_{Cs}(x) \cdot \frac{P(x,t) - 1}{T_1(x)} \quad (1)$$

where C_{Cs} - cesium concentration in mol·L^{-1}, P - instantaneous polarisation, t - time (in seconds), D_{Cs} - cesium spin diffusion coefficient (in A^2·s^{-1}), ∇ - the nabla operator, 1 (unity) - arbitrary equilibrium polarization, T_1 - spin-lattice relaxation time (in seconds) that depends on the spatial coordinate as:[3]

$$\frac{1}{T_1(x)} = \frac{1}{T_{1,dia}} + \frac{2}{15}\left(\frac{\mu_0}{4\pi}\right)^2 \frac{\gamma_{Cs}^2 g_e^2 \mu_B^2 S(S+1)}{x^6} \quad (2)$$

$$\cdot\left[\frac{\tau}{1+(\omega_n-\omega_e)^2\tau^2}+\frac{3\tau}{1+(\omega_n-\omega_e)^2\tau^2}+\frac{6\tau}{1+(\omega_n-\omega_e)^2\tau^2}\right]\stackrel{\text{def}}{=}\frac{K_1}{x^6}$$

where $T_{1,dia}$ - cesium spin-lattice relaxation time in the diamagnetic material ($CsPbBr_3$, in seconds), μ_0 - the vacuum permittivity, γ_{Cs} - the gyromagnetic ratio of ^{133}Cs, x - the distance between the cesium and the nearest paramagnetic Mn^{2+} atom, g_e - electron spin g-factor, μ_B - the Bohr magneton, τ - electronic correlation time, S - total electronic spin number (for Mn^{2+}, S = 5/2), and $\omega_{e/n}$ the electron/^{133}Cs Larmor frequency at 9.4 T.

The system follows initial and boundary conditions:

$$P(x,0) = 0 \tag{3}$$

and

$$\frac{\partial P}{\partial x}(x_{lim},t) = 0 \tag{4}$$

where x_{lim} corresponds to the position at the extremities of the system. Equation (3) corresponds to no initial polarization, since spins are all saturated at the beginning of the saturation-recovery experiment. Equation (4) corresponds to no flux at the edges of the system. It means that one side of the system represents the centre of the $CsMnBr_3$ cluster, and the other side of the system corresponds to a periodic boundary.

Is PRE relayed through ^{133}Cs-^{133}Cs spin diffusion?

De Gennes defined a pseudopotential ρ_1 to characterize the competition between the PRE effect and spin diffusion[4]:

$$\rho_1 = 0.68\left(\frac{K_1}{D_{Cs}}\right)^{1/4} \tag{5}$$

where K_1 - the PRE contribution from equation (2) and D_{Cs} - the cesium spin diffusion contribution. Physically, ρ_1 represents the distance from the electron at which spin diffusion and PRE exactly compensate each other. Beyond this ρ_1 distance, direct PRE is weak and thus any relaxation is coming from relayed PRE rather than direct PRE. Below this distance, the PRE effect is stronger and spin diffusion is too weak to relay it.

It means that if the pseudopotential ρ_1 is smaller than the length scale involved, spin diffusion will relay the PRE effect, and otherwise, the longitudinal PRE contribution will not be relayed.

In order to calculate ρ_1, we first need to calculate K_1 for manganese using equation (2). The only unknown for K_1 is τ. In order to find a value for τ, we calibrate equation (2) using the spin-lattice relaxation time measured for the diamagnetic reference, $CsMnBr_3$ ($T_{1,para}$ = 23 ms) for which 3 different Cs-Mn distances are involved, and known from the crystal structure: d_1 = 4.69 A, d_2 = 6.58 A, and d_3 = 8.95 A. Longer Cs-Mn distances are neglected due to negligible PRE due to the r^{-6} dependence. The resulting relaxation rate can be written as:

$$\frac{1}{T_1} = \frac{1}{T_{1,dia}} + \frac{K_1}{{d_1}^6} + \frac{K_1}{{d_2}^6} + \frac{K_1}{{d_3}^6} \quad (6)$$

The simulated build-up fits the experimental result best for τ = 350 ns:

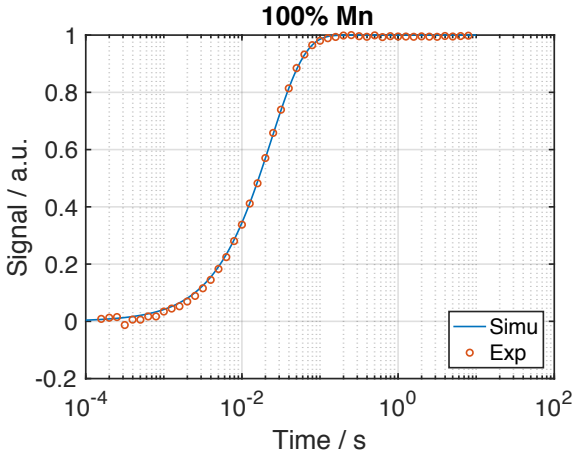

Figure S7. Experimental (circles) and simulated (solid line) ^{133}Cs build-up as a function of the recovery delay for $CsMnBr_3$ and a simulated correlation time of τ = 350 ns.

We can thus deduce the value for $K_1 = 3.9 \cdot 10^5$ A^6s^{-1}.

Now that K_1 is known, we calculate D_{Cs}. The cesium spin diffusion coefficient is estimated using the following equation:[2,5,6]

$$D_{Cs} = D_{PS} \cdot (C_{Cs}/C_H)^{1/3} \cdot (\gamma_{Cs}/\gamma_H)^2 \cdot \frac{1}{1 + k \cdot \nu} \quad (7)$$

where D_{PS} is the experimentally measured proton spin diffusion coefficient of polystyrene at 12.5 kHz at room temperature, D_{PS} = 7.5 10^3 $Å^2s^{-1}$,[7] C_{Cs} is the cesium concentration in the $CsPbBr_3$ lattice, C_{Cs} = 8.2 M, C_H the proton concentration in polystyrene, C_H = 70 M, $\gamma_{Cs/H}$ the cesium/proton gyromagnetic ratio, a scaling factor describing how the spin diffusion coefficient scales down with MAS (k = 0.6 ms),[6] and ν is the MAS spinning rate in kHz. Using these values, we find D_{Cs} = 4.9 10^{-2} $Å^2s^{-1}$ and thus ρ_1 = 36 Å. It means that ρ_1 is larger than the length scales involved. Indeed, the length scales involved here are the average Mn-Mn distances in a $CsPbBr_3$ lattice doped with 0.5%, 3%, and 8% Mn^{2+} which are 21.3 Å, 11.6 Å, and 8.4 Å, respectively. *This result demonstrates that PRE induced by Mn^{2+} is not relayed by ^{133}Cs-^{133}Cs spin diffusion.*

In the case of $MA_2Pb_xCo_{1-x}I_3$, is PRE relayed through ^{1}H-^{1}H spin diffusion?

Similar analysis applied to cobalt-doped $MAPbI_3$ (here S=3/2 for high-spin Co^{2+}) leads to τ = 0.9 ns, $K_1 = 1.2 \cdot 10^7$ A^6s^{-1}, D_H = 4.8 10^2 $Å^2s^{-1}$ and ρ_1 = 8.5 Å which shows that PRE induced by Co^{2+} *would indeed be relayed by spin diffusion*.

Consequences:
When PRE is **not** relayed by spin diffusion, we can neglect the effect of spin diffusion, and equation (1) becomes:

$$\frac{\partial P(x,t)}{\partial t} = -\frac{P(x,t) - 1}{T_1(x)} \tag{8}$$

which gives a simple solution: $P(x,t) = 1 - \exp\left(\frac{-t}{T_1(x)}\right)$

When PRE is relayed by spin diffusion, more complex solutions of equation (1) are found with numerical simulations, leading to the polarisation and signal curves analogous to those in Figure 4c-f.

Numerical solution to the bi-exponential saturation-recovery curves found for cobalt-doped $MAPbI_3$ lattice

No measurable ^1H PRE in the main perovskite phase and the clear bi-exponential behaviour of the curve in Figure 2d for 3% Co^{2+} in $MAPbI_3$ strongly suggests that cobalt is not incorporated into this phase. We confirm it by performing numerical simulations analogous to those described above. Figure S8 shows the vertical zoom of the fast relaxing component in the experimental and simulated build-ups. In the numerical simulation, we model spherical paramagnetic clusters (with $T_{1,para}$=6.7 ms) with different radii. Similarly as in Figure 4, we clearly see that if the cobalt were to form small clusters (1 nm radius, orange solid line), the PRE effect would be significant since the length scale involved here would be 5 nm, leading to stretched exponential relaxation behaviour. As we increase the radius of the simulated cluster, we see that a the behaviour become closer to bi-exponential since length scales become larger and the PRE effect becomes negligible. This situation fits the experimental data best. *This simulation allows us to conclude that the cobalt dopant is forming cobalt-rich clusters not smaller than 100 nm for 3% Co^{2+} doping.*

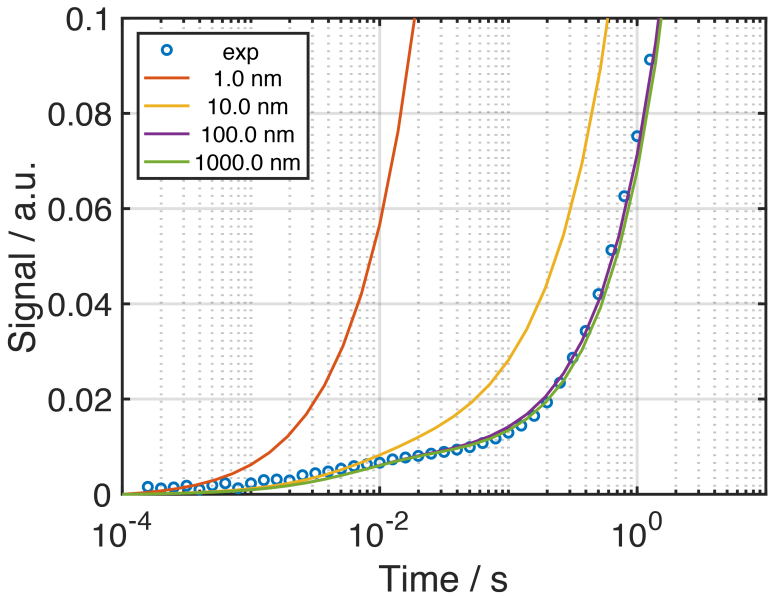

Figure S8. Experimental (blue circles) and simulated signal build-up (solid lines) as a function of the recovery delay for different cluster radii for $MAPb_{0.97}Co_{0.03}I_3$.

Relaxation data

The raw relaxation data for all the materials described in the main text can be found in the attached *raw_data.txt* tab-delimited text file.

References

(1) Daub Michael; Stroh Regina; Hillebrecht Harald. *Z. Für Anorg. Allg. Chem.* **2016**, *642*, 268–274.

(2) Bloembergen, N. *Physica* **1949**, *15*, 386–426.

(3) Bertini, I; Luchinat, C.; Parigi, G.; Ravera, E. *NMR of Paramagnetic Molecules*; Elsevier Science, 2017.

(4) de Gennes, P.-G. *J. Phys. Chem. Solids* **1958**, *7*, 345–350.

(5) G R Khutsishvili. *Sov. Phys. Uspekhi* **1966**, *8*, 743.

(6) Chaudhari, S. R.; Wisser, D.; Pinon, A. C.; Berruyer, P.; Gajan, D.; Tordo, P.; Ouari, O.; Reiter, C.; Engelke, F.; Copéret, C.; Lelli, M.; Lesage, A.; Emsley, L. *J. Am. Chem. Soc.* **2017**, *139*, 10609–10612.

(7) Roos, M.; Micke, P.; Saalwächter, K.; Hempel, G. *J. Magn. Reson.* **2015**, *260*, 28–37.